

## Article

# Cement Pastes with Hygroscopic Polymeric Additions for Potential Building Applications

Rosa Di Maggio \*, Gianluca Maracchini , Oscar Cotini  and Rossano Albatici 

Department of Civil, Environmental and Mechanical Engineering, University of Trento, Via Mesiano, 77, 38123 Trento, Italy; gianluca.maracchini@unitn.it (G.M.); oscar.cotini@unitn.it (O.C.); rossano.albatici@unitn.it (R.A.)

\* Correspondence: rosa.dimaggio@unitn.it

**Abstract:** The development of highly predictive analysis for designing cementitious composite with improved thermal and hygroscopic performance for building and construction poses a significant challenge. To investigate new potential applications, cement pastes have been prepared using a cement, sand, and crystallization admixture, with highly hygroscopic polymer additions (SA-PA) of sodium polyacrylate and/or recycled polyamide fibers. The porosity evolution was investigated at different curing stages and after heat treatment at 200 °C, the temperature at which the paste dehydrates quickly without structural changes. Mercury intrusion porosimetry (MIP), scanning electron microscopy (SEM), cyclic shear tests, thermal conductivity, and diffusivity measurements were carried out on the cement pastes to assess their microstructure. The behavior of the cement pastes varied with polymer additions and thermal treatments;  $ka^{-0.5}$  must be maximized in heat storage applications, where  $a$  and  $k$  are thermal diffusivity and conductivity, respectively. In contrast, the product  $a^{0.5}k^{-1}$  must be maximized in energy-efficient insulation. Cement pastes with SA-PA exhibited the highest values of both  $9.191 \cdot 10^2 \text{ m}^{-2} \text{ K}^{-1} \text{ s}^{0.5} \text{ W}$  and  $1.088 \cdot 10^{-3} \text{ m}^2 \text{ K s}^{-0.5} \text{ W}^{-1}$ , respectively. After the thermal treatment at 200 °C, SA-PA samples maintained the highest heat-storing performance of  $6.258 \cdot 10^2 \text{ m}^{-2} \text{ K}^{-1} \text{ s}^{0.5} \text{ W}$ , while the samples with SA-PA and polyamide fibers performed better in energy-efficient insulation, demonstrating performance of  $2.552 \cdot 10^{-3} \text{ m}^2 \text{ K s}^{-0.5} \text{ W}^{-1}$ . These results, discussed in terms of pore size distribution, suggest potential applications in the building field and are valuable for designing plaster and concrete for applications such as thermal and hygroscopic control.



**Citation:** Di Maggio, R.; Maracchini, G.; Cotini, O.; Albatici, R. Cement Pastes with Hygroscopic Polymeric Additions for Potential Building Applications. *Appl. Sci.* **2024**, *14*, 853. <https://doi.org/10.3390/app14020853>

Received: 12 December 2023

Revised: 10 January 2024

Accepted: 16 January 2024

Published: 19 January 2024



**Copyright:** © 2024 by the authors. Licensee MDPI, Basel, Switzerland. This article is an open access article distributed under the terms and conditions of the Creative Commons Attribution (CC BY) license (<https://creativecommons.org/licenses/by/4.0/>).

**Keywords:** pore size distribution; superabsorbent polyacrylate; polyamide fibers; thermal properties; eco-friendly retrofitting

## 1. Introduction

The demand for low-permeability concrete for building hydraulic structures, foundations, and under-pitch construction, and generally for water containment [1,2], has increased, prompting considerable study: the more impervious the concrete, the more durable the structure. Low-permeability concrete can reduce the degradation rate in chemically aggressive environments, the associated maintenance costs, and energy consumption [3–7]. A polymeric additive [8] could be a feasible solution to improve and tailor permeability; Jensen and Hansen proposed superabsorbent polyacrylate to achieve this aim [9]. In concrete, there are at least two different transport mechanisms: diffusion, due to a concentration gradient; and permeation, due to a pressure gradient between the two faces of a porous material [10]. In the latter case, the volume, size, and shape of pores are important [11–13]; the internal connection state changes with hydration reactions and crystallization. The mechanical strength of concrete correlates with permeability; therefore, pore distribution could indicate internal connectivity, which is useful in designing cementitious materials [14–17].

The porosity of concrete is mainly due to its cement paste, the binder of coarse aggregates. More frequently, cementitious materials, such as concrete, mortars, or plasters, contain polymeric fibers for structural use [18,19]: these additions affect the development of porosity. As recalled before, low permeability is linked to an absence of interconnected porosity: the larger the porosity, the greater the interconnectivity. In a previous study [20], a correlation was established between air permeability and the size of pores during the hydration of cement paste and the continuous growth of CSH crystals. Pore size distribution has been associated with water diffusion: the more CSH forms, the more gel pores, the fewer capillary pores, and the greater the strength. Moreover, it was also evidenced that the addition of superabsorbent poly-acrylates (SA-PA), as an internal curing additive [12,13], modifies the pore size distribution in cement paste; thus, a reduction in the capillary pressure and an improvement in the permeability was obtained.

The present study considered the effect of the addition of SA-PA and polyamide fibers (Ny) on the pore size evolution and the thermo-mechanical behavior of cement pastes, prepared using a cement mix containing a crystallization admixture. The latter was a calcium silicate, which hydrates quickly, forming crystalline seeds as nuclei for CSH crystallization and promoting the development of strength [20–23]. Aging progressively reduces the volume and size of pores; therefore, the presence of highly hygroscopic fibers or additions could induce a different pore distribution. SA-PA and Ny increase liquid permeation resistance because both absorb water, although to a different extent and, when simultaneously present, a mutual strengthening effect on porosity is supposed to occur [14]. Many factors could affect internal pore structures, including thermal treatment. In the present study, some samples were treated at 200 °C [24,25], the temperature at which cement paste, along with sodium polyacrylate [26], dehydrates quickly without giving rise to structural chemical transformations; in these conditions, however, polyamide fibers soften and flow, generating additional porosity. The pore size distribution is related to the cyclic response and subject to general load conditions, including partial unloading or reloading or mixed hysteretic loops [27] and thermal properties. The results of this study will provide new indications for designing new plaster/concrete for energy retrofitting, and more applications such as thermal insulation/storage. Emphasis has been recently placed on reducing energy consumption, the main action for a building energy retrofit, avoiding heat losses through infiltration [17]. Typical thermal insulating materials currently used for this purpose, such as polyurethane (PU), foamed polystyrene panels, or extruded polystyrene (EPS), may have significant environmental impact due to their high embodied carbon, which can delay the offsetting of their emissions, especially when aiming for near-zero-energy buildings. Thus, prolonged environmental breakeven periods (EBP) and increases in thermal discomfort could be observed, along with fire risk [28–33]. Accordingly, it is crucial to investigate the thermal saving contribution of new cementitious materials for plasters and coverings, also considering their possible applications for retrofitting historic and traditional massive walls [34].

## 2. Materials and Methods

### 2.1. Materials

Four different mixtures were prepared and tested during the early stage of aging. The samples were prepared by adding water to a pre-mixed powder, whose phases have been detailed in a previous paper [20], and then mixed for about 20 s. Although the technical data sheet of the pre-mixed powder provided by the manufacturer suggests a lower water/binder ratio for the preparation of the pastes,  $w/b = 0.4$  was used to attain manually workable pastes. Superadsorbent poly-acrylate (SA-PA) and/or nylon fibers (Ny) [20,35] were added to dry powder before mixing it with water.

The compositions of the four sets of cement mortars are summarized in Table 1. Notably, for mixtures with the same workability, the percentages of Ny and SA-PA were halved in the material containing both, with respect to the proportions each of them represented in the sample in which they were present alone. All the samples were prepared

using small quantities of mixture, not suitable for classic slump measurements. A spreading protocol was adopted: about 7.5 mL of mixture was poured into a cylinder 21 cm in diameter, vibrated for 30 s, and turned over onto a PET sheet, so that a diameter of about 5 cm could be measured.

**Table 1.** Percentage compositions of the samples.

Sample	Powder %	Water %	SA-PA %	Polyamide Fibers (Ny) %
CS	71	29	0.0	0.0
SA-PA	71	29	0.4	0.0
NY	69	29	0.0	2.3
NY/SA-PA	70	28	0.2	1.3

A single batch of commercial superabsorbent sodium polyacrylate (SA-PA) was used for all the experiments, accurately mixed before adding water, and then stirred for a few seconds before casting. The polymer was not brought to dryness, because being very hygroscopic it was preferred to use it in the condition reached in the jar already in equilibrium with the atmospheric humidity.

All the fresh pastes were cast into molds—polypropylene Petri dishes with 9 cm diameter and rubber molds of 1 cm × 1 cm × 0.3 cm—and vibrated for 30 s [20]. They were aged at different times at 20 ± 2 °C and R.H. 50 ± 5%. Each specimen was tested immediately after its curing process had been completed. In addition to the analyses carried out on fresh and cured samples, some pieces of the 28-day-aged samples were subjected to thermal treatment for further testing.

## 2.2. Characterization Methods and Instruments

A rotary viscometer was used to carry out viscosity measurements on fresh mortars with and without additions. The instrument was powered by a crank that drove a spindle through the precision gear. The shift cam selected fixed speeds. A knob on the gear cam hub determined the force of the fluid. The viscosity measurements of the instrument ranged from 1 to 6.106 mPa·s, changing the spindle diameter from large to thin, respectively. Due to the changes in viscosity being too fast, which prevented the measurement of stable values, the times that the cement pastes took to reach a viscosity value of 390 mPa·s were measured.

Porosity was measured through Hg intrusion on fragments that were put into the chamber of the porosimeter. Under a vacuum, the chamber was filled with mercury [36], which penetrated the open porosity of the solid due to the increasing application of pressure. By measuring the quantity of mercury that had penetrated the pores at each pressure increase, the cumulative volume was obtained as a function of the pore radius [37,38].

The mechanical properties were analyzed using dynamic mechanical spectroscopy (DMS) in shear configuration. A 5000 mN force was applied at a 500 mN/min rate in five load/unload cycles. To obtain samples of an appropriate size, pastes were cast in rubber molds of 1 cm × 1 cm × 0.3 cm. Unfortunately, the thicknesses of the samples were not measured with a caliper each time. For this reason, the precise resistant section is not known, and could vary in a range ±0.5 mm; the error in determining the shear stress could be very large.

The samples underwent an isothermal treatment for 1 h at 200 °C, after 28 days of aging at 95% relative humidity. The samples were weighed before and after the treatment.

The thermal properties of samples were measured with a hot disk, using the transient plane source technique (TPS). The tests were carried out at room temperature using different Kapton insulated sensors (2.001 to 6.403 mm radius) with a nickel double spiral. During the test, an electric flow passes through the sensor, increasing the temperature of the samples at different heat rates depending on the heat transfer properties of the specimen. In this specific case, a thermal power of 10 to 50 mW was supplied for 5 to 20 s.

Scanning electron images of samples during and after 28 days of curing were acquired on samples prepared without any polishing to avoid contamination, and then coated with gold.

### 3. Results and Discussion

#### 3.1. Rheological Observations

When the powder was mixed with water, a great amount of heat was released and the fresh mixtures became less fluid. This change occurred too fast for stable viscosity values to be measured. Instead, the times that the cement pastes took to reach a viscosity value of 390 mPa·s were measured, as shown in Table 2. Accordingly, CS required 17 s to reach 390 mPa·s; SA-PA required just 11 s. Sodium polyacrylate made the paste less fluid, because water was rapidly absorbed by the hygroscopic addition and subtracted from its rheological role. The times measured for samples containing fibers were so low as to be unreliable; the rapid loss of workability probably resulted from the incorporation of the fibers into the cement paste during mixing. These aspects are essential when a forming technique (laying, casting, or extrusion) must be chosen: the rheology of the mixture should be constant at least for the time necessary to complete the process. This is therefore not the case for mixtures containing crystallization additives. Moreover, 3D printers, which are mostly software-controlled extruders, are currently not suitable for forming such pastes.

**Table 2.** Times that fresh samples needed to reach a viscosity limit of 390 mPa·s at a rate of 1.5.

Sample	Time (s)
CS	17 ± 1
SA-PA	11 ± 1
NY	5 ± 2
NY/SA-PA	5 ± 3

#### 3.2. Porosity Distribution

The graphs in Figure 1 show the averages of three porosity distributions for each sample during aging (the first three rows at 3, 14, and 28 days, respectively) and after a 200 °C thermal treatment of samples aged for 28 days. After the thermal treatment, all the samples exhibited significant weight loss [23,24] due to water evaporation, as detailed in Table 3.

**Table 3.** Weight loss percentages of samples cured for 28 days after the thermal treatment at 200 °C and the total porosity percentages.

Sample	Total Porosity after 3 Days of Aging (%)	Total Porosity after 14 Days of Aging (%)	Total Porosity after 28 Days of Aging (%)	Total Porosity after 28 Days of Aging and after the Thermal Treatment at 200 °C for 1 h (%)	Weight Loss after 28 Days of Aging and after the Thermal Treatment at 200 °C for 1 h (%)
CS	16 ± 2	19 ± 3	29 ± 1	36 ± 1	27 ± 1
SA-PA	18 ± 3	29 ± 1	32 ± 2	41 ± 1	27 ± 1
NY	24 ± 5	20 ± 2	20 ± 2	43 ± 1	28 ± 2
NY/SA-PA	17 ± 1	20 ± 3	23 ± 1	41 ± 2	26 ± 2

After 3 days of curing, the distribution of CS mainly consisted of mesopores, which had widths between 2 and 50 nm [39]. Microporosity increased with curing time and thermal treatment. Both the additions, SA-PA and fibers, increased the number of macropores, ensuring that permeability increased with curing and even after thermal treatment. It is already known that the macroporosity of SA-PA is higher compared with CS samples [1,38], but macropores increase even more in the presence of polyamide fibers (NY/SA-PA). Macropores must also be due to the less homogeneous and workable paste, as observed

during viscosity measurements; this lets air remain entrapped around fibers. The number of mesopores decreased during aging for all the samples and even after thermal treatments, but the size distribution was asymmetrical toward larger sizes. The samples containing fibers showed a bimodal pore distribution, with micropores (having widths  $< 2$  nm [39]) and macropores (having widths  $> 50$  nm [39]). This bimodal distribution maintains with aging and even after the heat treatment at  $200$  °C, if SA-PA is present. Macropores allow internal core access and prevent the growth of pore pressure. Macrovoids could also increase by softening and flowing of fiber, whereas SA-PA residuals absorb diffusing water. Accordingly, the pore distribution data, obtained from MIP measurements, confirmed these mixtures as a strong tool to investigate the evolution of paste microstructures during aging and after thermal treatment.

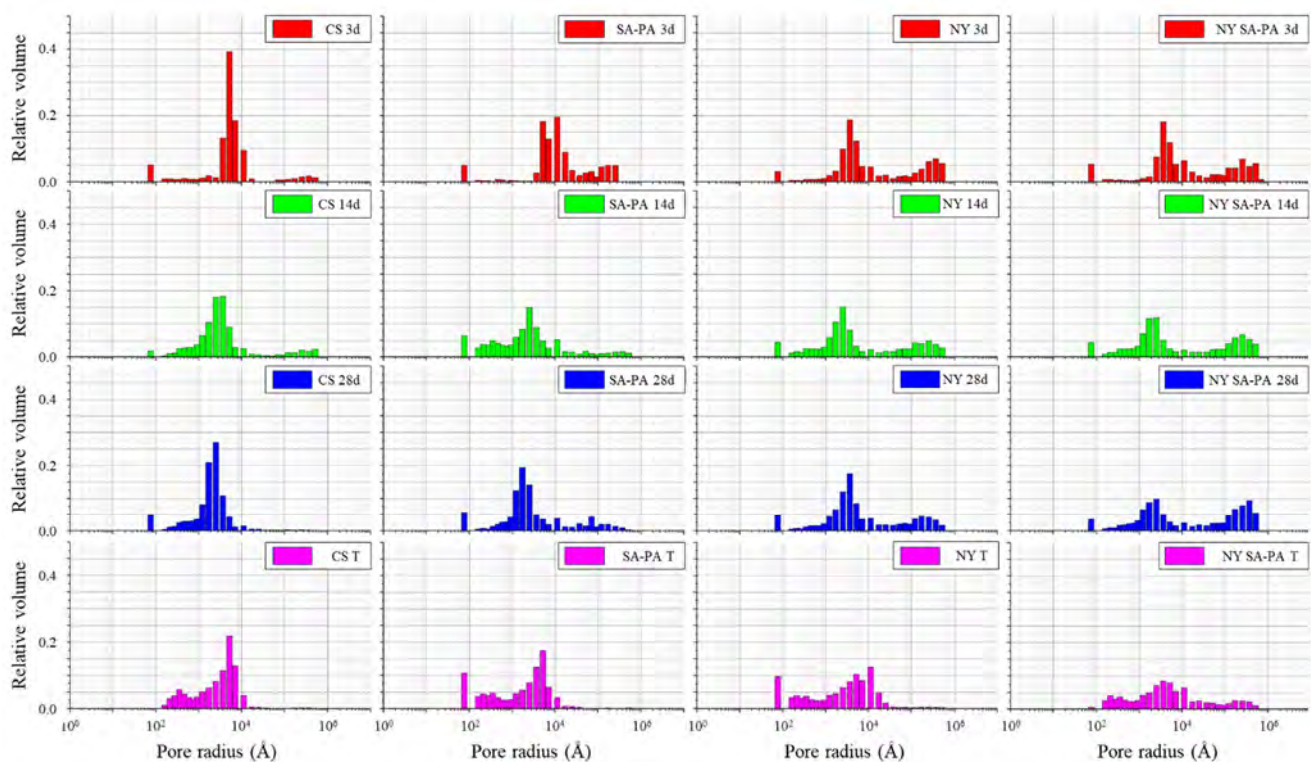


**Figure 1.** Porosity distribution during the first 28 days of aging and after thermal treatment.

### 3.3. SEM Observations

SEM observations (Figures 2 and 3) on the samples containing nylon fibers (NY and NY/SA-PA) after 3 and 28 days of aging showed the presence of large empty cavities, especially at the fiber–matrix interface: fibers did not adhere well to the matrix in the early stages of aging, and the cavities were too large to be completely closed by CSH crystal growth. The chemical interactions between the cement paste and polyamide fibers were poor [40]. The great amount of water (up to 12% wt) absorbed on the fibers' surface, due to the highly polar hydroxyl and amide functional groups [41], influenced the interconnection with porosity much more than polymeric fibers typically used for reinforcement, such as polyethylene (PE) or polypropylene (PP). Moreover, observing Figures 2 and 3, it can be noted that crystals are everywhere, but are small and not interconnected; the presence of highly hygroscopic addition seemed to have stopped crystallization after the contact between the water and powder mix. The observed crystals were those nuclei formed by the crystallization admixture during mixing. Water, absorbed by fibers, was subjected to crystallization and then evaporated due to its associated porosity. The addition of both fibers and polyacrylate, albeit in half the proportions, increased the removal of water from

the cement hydration. Accordingly, the stiffness of NY/SA-PA subjected to the same aging was hypothesized to be lower than that of NY.

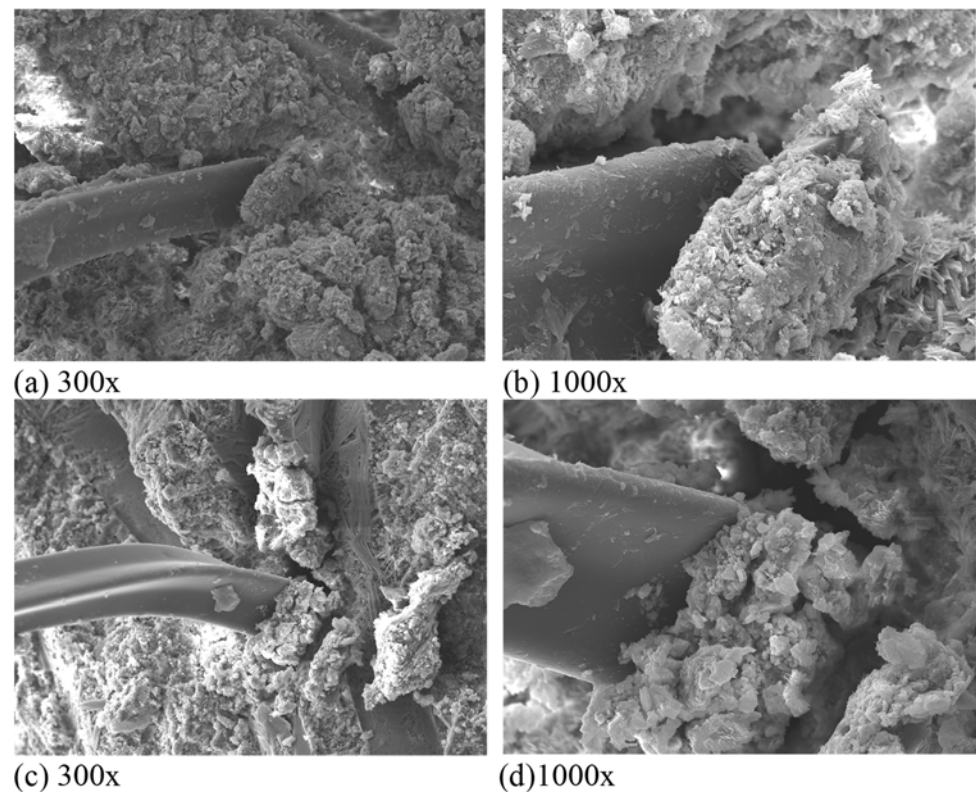


**Figure 2.** SEM micrographs of 3-day-aged (a,b) and 28-day-aged (c,d) NY samples.

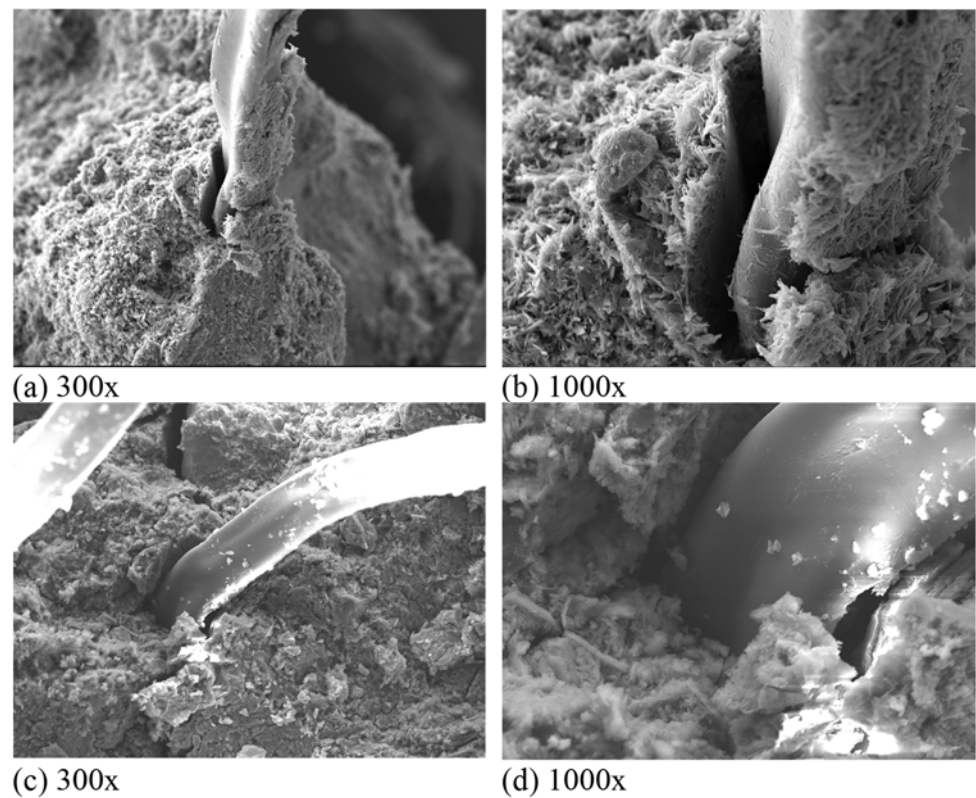


**Figure 3.** SEM micrographs of 3-day-aged (a,b) and 28-day-aged (c,d) NY/SA-PA samples.

The samples without SA-PA and CS fibers (Figures 4 and 5, respectively) appeared well crystallized. SA-PA absorbed water during mixing, but released it slowly during the hydration of the cement phase, which was continuous and homogeneous, without the formation of large empty cavities.

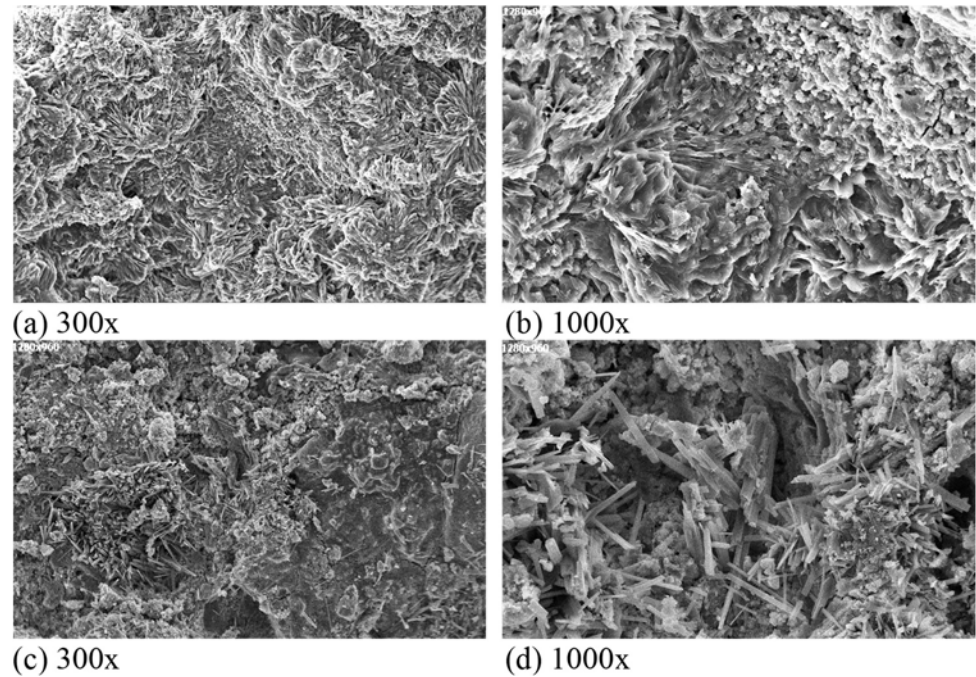


**Figure 4.** SEM micrographs of 3-day-aged (a,b) and 28-day-aged (c,d) SA-PA samples.

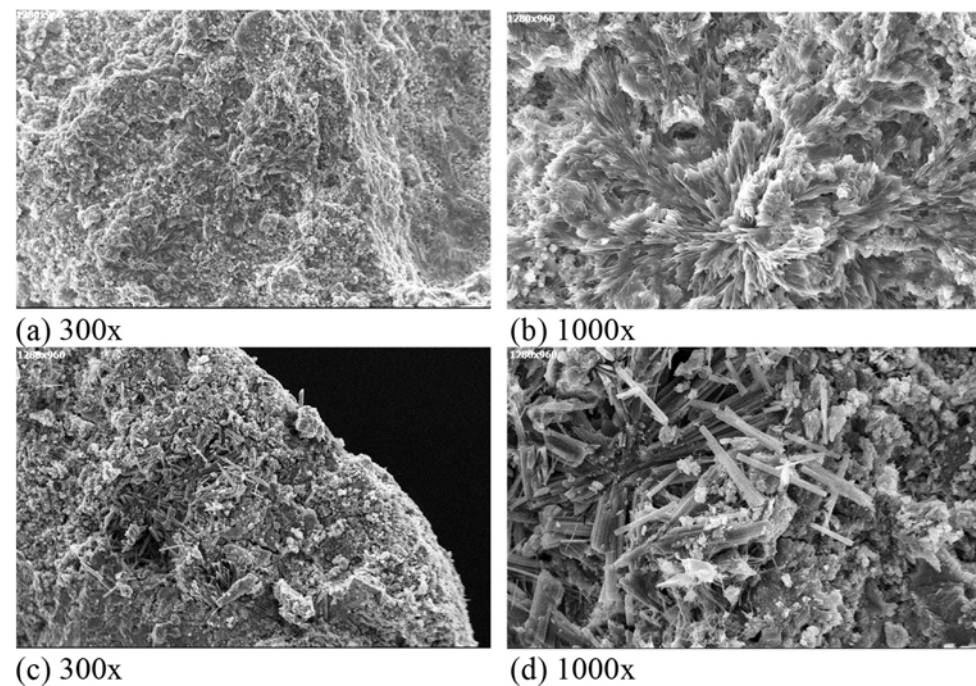


**Figure 5.** SEM micrographs of 3-day-aged (a,b) and 28-day-aged (c,d) CS samples.

### 3.4. Mechanical Tests

To gain further insight into the response of cement pastes under shear loading/unloading cycles, tests were carried out on small prismatic specimens. Each test consisted of five cycles; Figure 6a–c shows the load–displacement curve (maintaining the same

abscissa). The presence of a hysteresis loop suggests the occurrence of anelastic phenomena. The area of each hysteresis cycle is proportional to the energy dissipated during each loading–unloading cycle. All the curves started from zero (stress–strain), but none returned to zero, maintaining a permanent strain (non-recoverable strain); this depended on the curing time, additions, and of course, the previous loading history [26]. After three days (Figure 6a), the amount of energy dissipated in each cycle was very small. This suggests that the stiffness of each sample was maintained high for the entire stress–strain test. The stiffest materials were those with fibers and the most deformable were CS and SA-PA after seven days of aging. These plots are not shown. This behavior is neither strange, nor was it unexpected. In a previous paper [20], it was reported that cement paste prepared with a crystallization mixture is more permeable after seven days than after three days of aging, due to the evaporation of water when the crystallization of cement phases is far from complete. On the other hand, polyacrylate acts as a plasticizer in cement paste, absorbing water and always retaining at least a small amount of it.

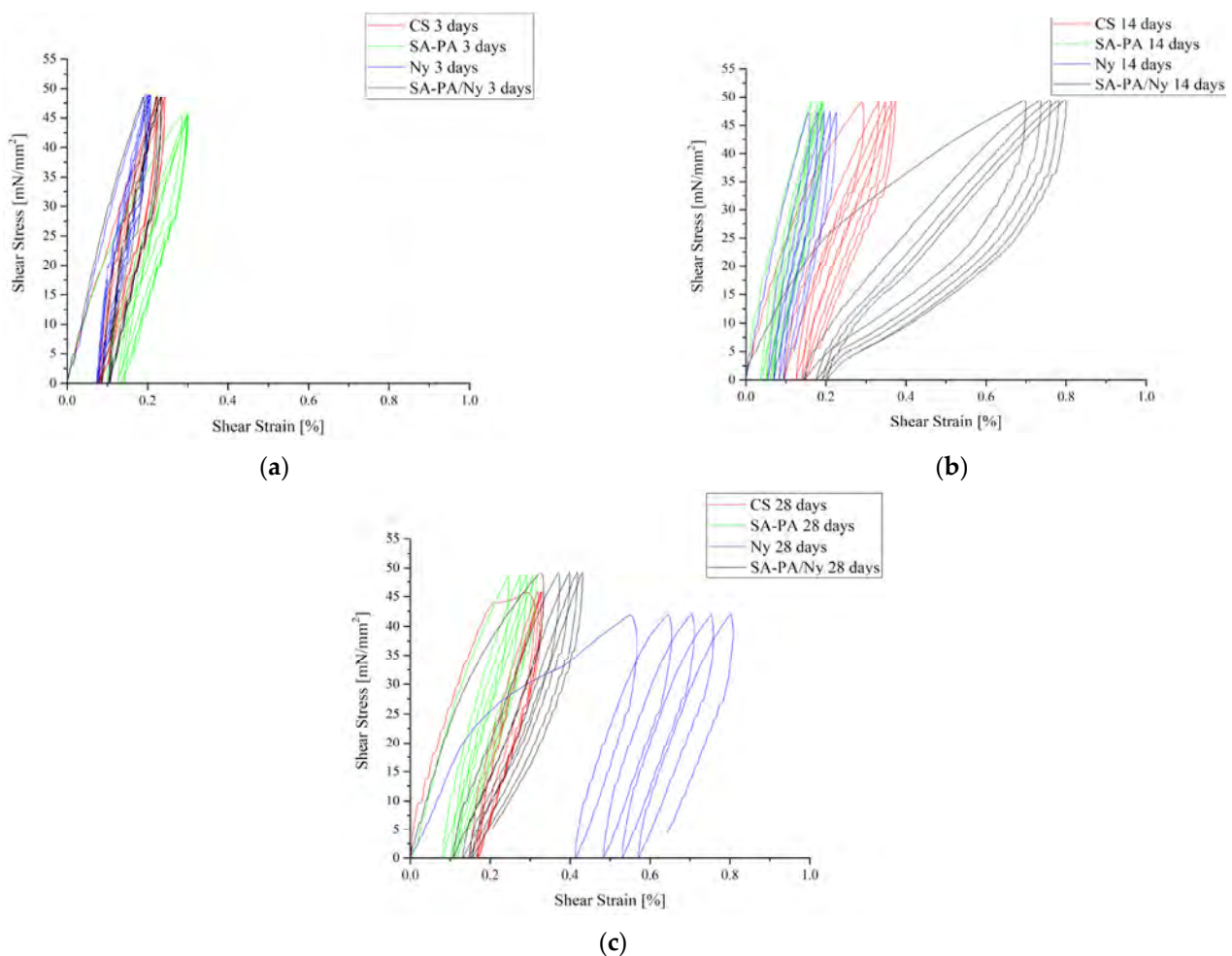


**Figure 6.** Loading–unloading shear stress–shear strain (%) curves at different curing times: 3 days (a), 14 days (b), and 28 days (c).

After 14 days of aging, the deformability of all the samples increased. SA-PA/Ny not only showed an increase in permanent strain with each loading and unloading cycle, but also exhibited an increasing maximum strain: every time the sample was unloaded, the next cycle moved to higher maximum deformation, even if the sample regained almost the first permanent deformation. In Figure 6b, the unloading and the reloading paths of the SA-PA/Ny sample are significantly different, exhibiting large hysteresis loops. The curves of the 14-day-aged samples showed an inflection point on unloading. This could be

an indicator of crack development in the material [42]. Degradation of the concrete was reflected in the decrease in the slopes of the reloading curves. Reloading curves were nearly linear, up to the beginning of the unloading curve, after which softening could be observed. The unloading curve softened gradually while the stress decreased and the stiffness of the unloading curve became smaller.

After 28 days of aging, all the materials appeared to be stiff (see Figure 6c), except for NY. The latter exhibited considerable permanent deformation which increased every cycle, while the hysteresis loop did not increase at all. The number of microcracks in the paste was expected to increase sharply. As a result, undamaged portions that carried the load were reduced and the stress–strain relationship became even more non-linear. The residual strains were a function of the strain at unloading. An increase in unloading strain caused approximately the same increase in the accumulated residual strain. The differences from the other samples were mainly due to the extent of crystallization of the cement paste, which, in turn, depends on the degree of porosity and viscous deformation.

In Figure 7a–d, the evolution of the shear stress/shear strain curves during aging (3, 14, and 28 days) for each type of sample is shown. As the aging increased, the viscous deformation of all the samples decreased progressively, but this could not occur at the same rate or achieve the same final properties. As aging increased, the viscous deformation of all the samples was expected to decrease progressively, but this could not occur at the same rate, achieving the same final properties. Notably, after 28 days, the Ny sample still demonstrated a viscous plastic behavior, whereas SA-PA/Ny already appeared more rigid, even if less than the CS and SA-PA samples. The differences are clearly depicted in Figure 8a–d. These figures show all the hysteresis cycles, comprehensively illustrating the measure of dissipated energy, and consequently, the degree of deformation of each type of sample. The larger the hysteresis cycle, the more voids are suitable for modification in an iso-enthalpic way. This depends on the reconfiguration of empty pores in a material that cannot crystallize well due to water shortages. Sodium polyacrylate is the most efficient source of slow and continuous release of water for cement crystallization. Polyamide fibers are also a source of water, but they contribute less than polyacrylate to a slow water release during aging since their surfaces absorb up to 10–12% by weight, but above all, as observed in the SEM images, because large voids form at the interface fiber–matrix due to poor interactions.

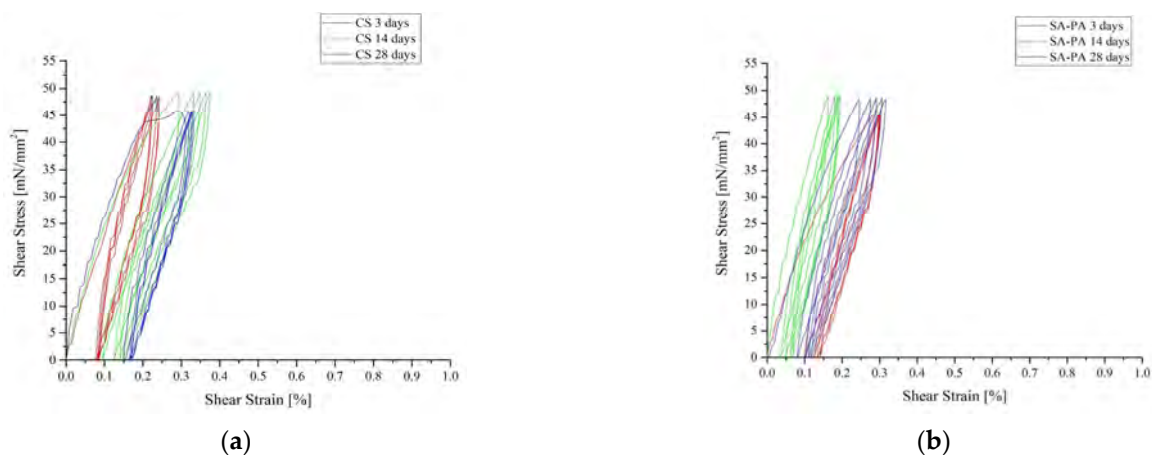
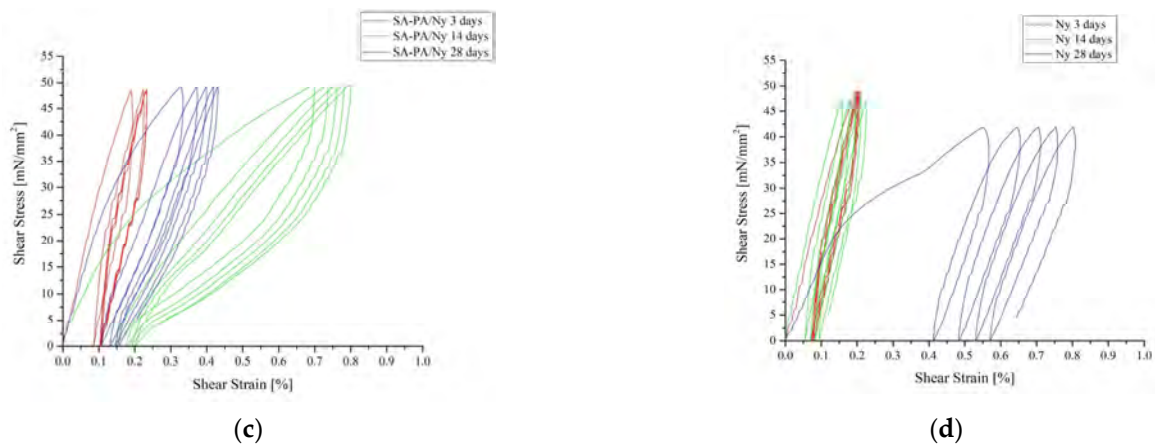
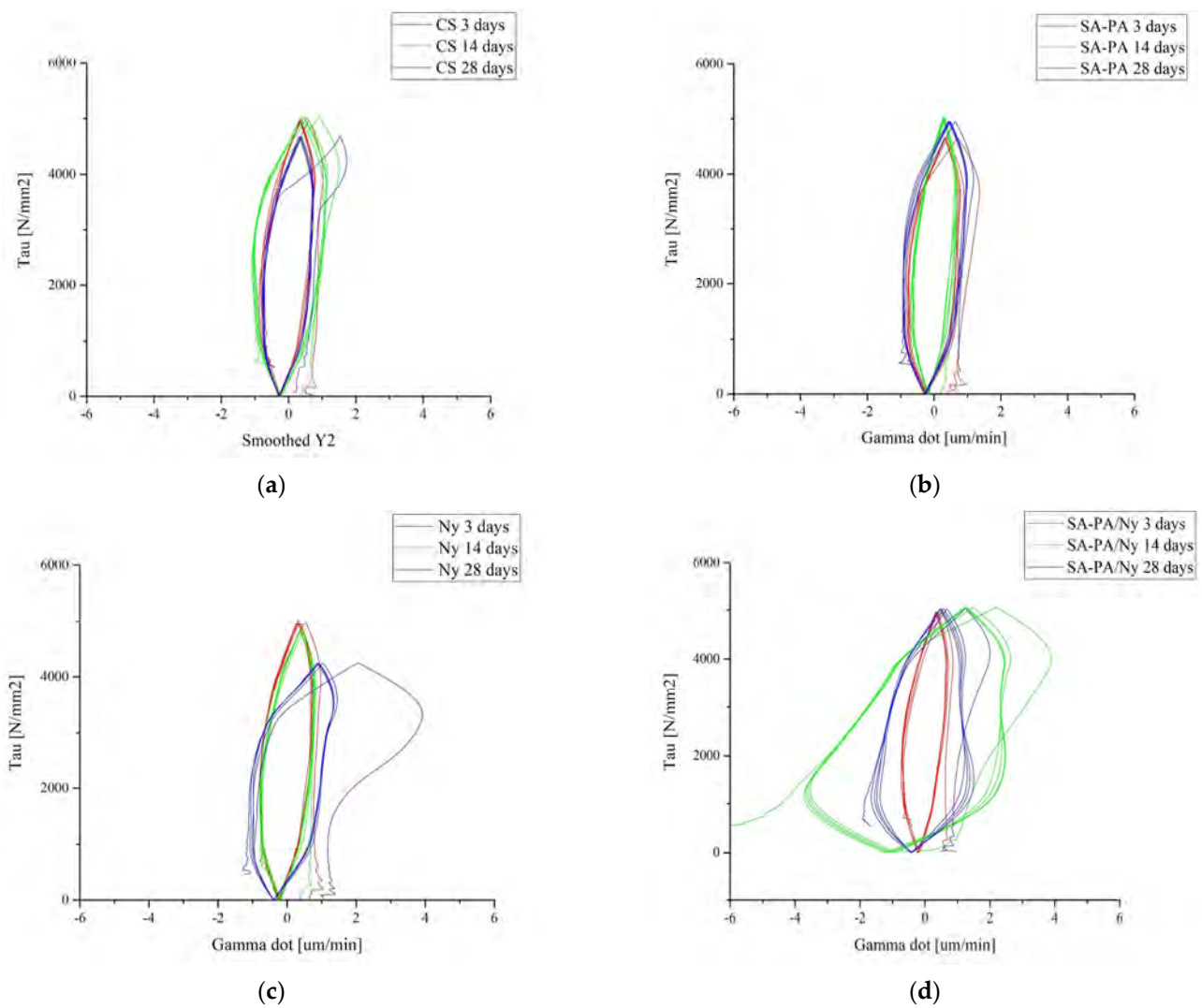


Figure 7. Cont.



**Figure 7.** Stress–strain curves of CS (a), SA-PA (b), Ny (c), and Ny/SA-PA (d) after 3, 14, and 28 days of curing.



**Figure 8.** Shear stress–shear strain rate curves of CS (a), SA-PA (b), Ny (c), and Ny/SA-PA (d) after 3, 14, and 28 days of curing.

### 3.5. Thermal Measurements

Cementitious pastes could also be eligible for solar storage walls or to reduce energy loss during heating cycles in buildings [43–45]. Table 4 shows the thermal properties of the 28-day-aged samples before and after thermal treatment, during which the release of bonded water may have occurred in cement paste. Accordingly, the thermal conductivity decreased with water content, as expected [23]. Notwithstanding, all the thermal conductivity values after the 200 °C thermal treatment were above 0.3 W/mK, the required value indicated in the literature for high-temperature concrete [46,47]. According to the following equation,  $dQ/dt = -kA dT/dt$ , thermal conductivity ( $k$ ) is the most important physical property, which guarantees a rapid and complete charge/discharge cycle of a thermal storage unit [43–49]. A cement paste for plaster could preferably be used for improving the comfort of a building, reducing energy consumption through a heat-storing element for passive solar heating. In that case, thermal diffusivity ( $a$ ) is critical, and the product ( $ka^{-0.5}$ ) must be maximized. In contrast, when a material is required to work as an energy-efficient element for thermal insulation and minimizing wasted energy in a heating cycle,  $a^{0.5}k^{-1}$  must be maximized, to exemplify the improved diffusivity [43,44]. Conductivity governs the heat flow through a material in steady state, while diffusivity determines the transient heat flow. Moreover, the density of porous materials is very low, so the thermal conductivity is low, although their thermal diffusivity is not necessarily low; they may not transmit much heat and reach a steady state quickly. In addition to density and heat capacity, conductivity depends on the average speed and distance of electrons and/or phonons [43]. Foams and porous materials have low conductivity because the motion of gas is restricted in the porosity and no free electrons and/or phonons are present. Instead, foams, having a low mass (and therefore a low heat capacity), have great diffusivity and short-term insulation capacity (i.e., the ability to maximize the time before the inside temperature changes after the outside temperature has suddenly changed) [43].

**Table 4.** Thermal properties of the 28-day-cured samples acquired with the hot disk instrument in addition to the values of  $ka^{-0.5}$  and  $a^{0.5}k^{-1}$ , which indicate the material's eligibility for heat storage and insulation, respectively.

		Thermal Conductivity (k) (W/mK)	Thermal Diffusivity (a) (mm <sup>2</sup> /s)	Specific Heat (MJ/m <sup>3</sup> K)	$k/a^{0.5}$ (m <sup>-2</sup> K <sup>-1</sup> s <sup>0.5</sup> W)	$a^{0.5}/k$ (m <sup>2</sup> K s <sup>-0.5</sup> W <sup>-1</sup> )
No Treatment	CS	0.880	0.304	2.892	$1.596 \cdot 10^3$	$6.267 \cdot 10^{-4}$
	SA-PA	0.711	0.599	1.187	$9.191 \cdot 10^2$	$1.088 \cdot 10^{-3}$
	NY	0.800	0.329	2.431	$1.395 \cdot 10^3$	$7.171 \cdot 10^{-4}$
	NY/SA-PA	0.850	0.356	2.387	$1.424 \cdot 10^3$	$7.022 \cdot 10^{-4}$
200 °C (1 h)	CS	0.394	0.720	0.547	$4.640 \cdot 10^2$	$2.155 \cdot 10^{-3}$
	SA-PA	0.351	0.314	1.118	$6.258 \cdot 10^2$	$1.598 \cdot 10^{-3}$
	NY	0.326	0.352	0.926	$5.491 \cdot 10^2$	$1.821 \cdot 10^{-3}$
	NY/SA-PA	0.341	0.756		$3.918 \cdot 10^2$	$2.552 \cdot 10^{-3}$

Both the values of  $ka^{-0.5}$  and  $a^{0.5}k^{-1}$  are shown in Table 4, calculated for each sample from the measured values of  $a$  and  $k$ . Among the samples aged for 28 days, SA-PA samples maximized the values of both products. Accordingly, SA-PA samples could have the best performance both if used in heat-storing walls (i.e., the sun shines on the outside during the day and the wall stores heat, which is extracted at night) and in energy-efficient elements for thermal insulation (i.e., to minimize the energy consumed in each heating cycle; turning the heat on, the equivalent of heat capacity of the walls should supply them) [43,44]. This result could be attributed to the highest value of thermal diffusivity.

When heated, cementitious material releases water vapor that increases the pressure of the pores and lowers the diffusivity. To keep diffusivity high, a cementitious material

must comprise interconnected pores, so that the water vapor can be distributed. The bimodal pore size distribution of the SA-PA samples suggests that small pores, optimizing thermal diffusivity, are numerous and interconnected by a few macropores. Accordingly, the specific heat is low (Table 4). As already discussed, polyamide fibers create large voids at the fiber–matrix interface, along which water vapor comes out easily.

Among the samples treated at 200 °C, CS and NY/SA-PA showed the highest value of diffusivity and the best behavior in heating cycle insulating. All the treated samples, having already lost a lot of water during the thermal treatment, exhibited a lower specific heat than the same samples not thermally treated. Table 3 also shows the percentages of total porosity, which increased after the heat treatment, although the absolute values cannot be directly compared. As already known [15,16,20], the percentage of porosity alone is not sufficient to describe the behavior of a cementitious material as much as the pore size distribution, along with the overall water content. The NY/SA-PA sample, having lost one percentage point less than the other samples, contained moisture that must still have been able to move, benefiting from the macroporosity.

#### 4. Conclusions

Four sets of cement pastes were prepared with a commercial premix containing calcium silicates, quartz, and a crystallization admixture, which accelerated the strength development rate. Three sets were prepared with hygroscopic polymer additions of sodium polyacrylate (SA-PA) and/or recycled polyamide fibers (NY) to study the evolution of their pore size distribution, shear mechanical response, and thermal properties at different aging times and after thermal treatment at 200 °C. From the study, it was hypothesized that the behavior of cement pastes depends on the type of polymeric addition; the conclusions are listed below.

1. Hygroscopic polymeric additions make cement paste less workable than CS, because they rapidly absorb water, detracting from its rheological role.
2. The porosity evolution was investigated at different curing stages; mercury intrusion porosimetry (MIP) has been used for investigating pores' evolution during aging and after a heat treatment at 200 °C. The pore size distribution appeared to be bimodal when sodium polyacrylate was added, as already reported in the literature [20]. The presence of polyamide fibers made the pore size distribution bimodal. This distribution was maintained during aging for up to 28 days. NY/SA-PA was the only sample that maintained the bimodal distribution even after the heat treatment.
3. Under five cycles of loading–unloading shear stress, the samples containing polyamide fibers showed significant visco-plastic deformation until pores cracked at the tip and connected with adjacent pores to form a micro-fracture surface. The micro-fracture surface extended, forming macroscopic cracks, which could eventually lead to shear failure of the cement paste consolidation body along the interface layer.
4. Cement pastes are useful for heat-storing walls or energy-efficient insulation. In the first case, the product  $ka^{-0.5}$ , where  $k$  is the thermal conductivity and  $a$  is the thermal diffusivity, must be maximized, whereas  $a^{0.5}k^{-1}$  must be maximized in the second case. The cement paste containing sodium polyacrylate (SA-PA sample) maximized both values ( $9.2 \cdot 10^2 \text{ m}^{-2} \text{ K}^{-1} \text{ s}^{0.5} \text{ W}$  and  $1.1 \cdot 10^{-3} \text{ m}^2 \text{ K s}^{-0.5} \text{ W}^{-1}$ , respectively) due to its high diffusivity. After thermal treatment at 200 °C, SA-PA showed the highest value for heat-storing ( $6.3 \cdot 10^2 \text{ m}^{-2} \text{ K}^{-1} \text{ s}^{0.5} \text{ W}$ ), whereas the sample containing both nylon fibers and sodium polyacrylate (Ny/SA-PA sample) showed the highest values for energy-efficient insulation ( $2.6 \cdot 10^{-3} \text{ m}^2 \text{ K s}^{-0.5} \text{ W}^{-1}$ ) due to the concurrent presence of macro- and micropores.
5. Further studies will be necessary to confirm the trends in pore distribution and the effects on thermal and mechanical properties. Future research should also consider other cementitious materials to increase the predictive indications for designing large-scale concrete, plaster, coatings, or mortar.

**Author Contributions:** Conceptualization, R.D.M., R.A. and G.M.; methodology, O.C.; software, O.C.; validation, R.D.M., G.M. and R.A.; formal analysis, R.D.M. and O.C.; investigation, O.C.; resources, R.A., R.D.M. and G.M.; data curation, R.D.M.; writing—original draft preparation, R.D.M. and O.C.; writing—review and editing, R.D.M. and G.M.; visualization, G.M.; supervision, R.A.; project administration, R.D.M.; funding acquisition, R.D.M., R.A. and G.M. All authors have read and agreed to the published version of the manuscript.

**Funding:** This research received no external funding.

**Data Availability Statement:** The raw data supporting the conclusions of this article will be made available by the authors on request.

**Acknowledgments:** The binder called “Concentrate Xypex”—PROBAR XYPEX was provided by PROBAR Italia (Comano, Milan, Italy). W. Vaona is acknowledged for the preparation of samples and SEM observations. V. M. Sglavo and L. Zottele are acknowledged for performing porosity measurements using the Hg intrusion porosimeter.

**Conflicts of Interest:** The authors declare no conflicts of interest.

## References

- Longhi, F.; Surico, F. Effect of a Crystallizing Admixtures on Concrete Properties: Italian Concrete Days. In Proceedings of the Conference on Italian Concrete Days, Naples, Italy, 14–17 April 2021; Springer: Berlin, Germany, 2018; pp. 312–324.
- Coppola, L.; Coffetti, D.; Crotti, E. Innovative carboxylic acid waterproofing admixture for self-healing watertight concrete. *Const. Build. Mater.* **2018**, *171*, 817–824. [[CrossRef](#)]
- Cui, L.; Cahyadi, J.H. Permeability and pore structure of OPC paste. *Cem. Conc. Res.* **2001**, *31*, 277–282. [[CrossRef](#)]
- Muhammad, N.Z.; Keyvanfar, A.; Majid, M.Z.A.; Shafaghat, A.; Mirza, J. Waterproof performance of concrete: A critical review on implemented approaches. *Constr. Build. Mater.* **2015**, *101*, 80–90. [[CrossRef](#)]
- Wang, W.; Wang, S.; Yao, D.; Wang, X.; Yu, X.; Zhang, Y. Fabrication of all dimensional superhydrophobic mortar with enhanced waterproof ability and freeze-thaw resistance. *Constr. Build. Mater.* **2020**, *238*, 117626. [[CrossRef](#)]
- Li, C.; Wu, M.; Chen, Q.; Jiang, Z. Chemical and mineralogical alterations of concrete subjected to chemical attacks in complex underground tunnel environments during 20–36 years. *Cem. Concr. Compos.* **2018**, *86*, 139–159. [[CrossRef](#)]
- Li, J.; Jin, Q.; Zhang, W.; Li, C.; Monteiro, P.J.M. Microstructure and durability performance of sustainable cementitious composites containing high-volume regenerative biosilica. *Resour. Conserv. Recycl.* **2022**, *178*, 106038. [[CrossRef](#)]
- Di Maggio, R.; Dirè, S.; Callone, E.; Bergamonti, L.; Lottici, P.P.; Albatici, R.; Rigon, R.; Ataollahi, N. Super-adsorbent polyacrylate under swelling in water for passive solar control of building envelope. *SN Appl. Sci.* **2020**, *2*, 45. [[CrossRef](#)]
- Jensen, O.M.; Hansen, P.F. Water-entrained cement-based materials: I. Principles and theoretical background. *Cem. Concr. Res.* **2001**, *31*, 647–654. [[CrossRef](#)]
- Hu, J.; Stroeven, P. Local porosity analysis of pore structure in cement paste. *Cem. Concr. Res.* **2005**, *35*, 233–242. [[CrossRef](#)]
- Reinhardt, H.W.; Gaber, K. From pore size distribution to an equivalent pore size of cement mortar. *Mater. Struct.* **1990**, *23*, 3–15. [[CrossRef](#)]
- Guo, Y.; Zhang, P.; Ding, H.; Le, C. Experimental Study on the Permeability of SAP Modified Concrete. *Materials* **2020**, *13*, 3368. [[CrossRef](#)]
- Rose, D.A. Water movement in unsaturated porous materials. *RILEM Bull.* **1965**, *2912*, 119–124.
- Fu, J.-X.; Wang, K.; Wang, J. Internal pore evolution and early hydration characterization of fly ash cement backfill. *J. Build. Eng.* **2023**, *72*, 106716. [[CrossRef](#)]
- Stazi, F.; Corinaldesi, V.; Capotondo, Y.; Porcarelli, I.; Di Perna, C.; D’Orazio, M. Effect of pore modulating additives-sepiolite and colloidal nano silica on physical, mechanical and durability properties of lime-based renders. *Mater. Struct.* **2022**, *55*, 123. [[CrossRef](#)]
- Isebaert, A.; De Boever, W.; Descamps, F.; Dils, J.; Dumon, M.; De Schutter, G.; Van Ranst, E.; Cnudde, V.; Van Parys, L. Pore-related properties of natural hydraulic lime mortars: An experimental study. *Mater. Struct.* **2016**, *49*, 2767–2780. [[CrossRef](#)]
- Liu, X.; Chen, X.; Shahrestani, M. Optimization of Insulation Thickness of External Walls of Residential Buildings in Hot Summer and Cold Winter Zone of China. *Sustainability* **2020**, *12*, 1574. [[CrossRef](#)]
- Mercuri, M.; Vailati, M.; Gregori, A. Lime-based mortar reinforced with randomly oriented polyvinyl-alcohol (PVA) fibers for strengthening historical masonry structures. *Dev. Built Environ.* **2023**, *14*, 100152. [[CrossRef](#)]
- Zhang, X.; Du, M.; Fang, H.; Shi, M.; Zhang, C.; Wang, F. Polymer-modified cement mortars: Their enhanced properties; applications; prospects, and challenges. *Constr. Build. Mater.* **2021**, *299*, 124290. [[CrossRef](#)]
- Cotini, O.; Di Maggio, R.; Tonelli, D.; Nascimben, R.; Ataollahi, N. Porosity of a fast-setting mortar with crystallization admixture and effect of a SA-PA modification. *Materials* **2022**, *15*, 1542. [[CrossRef](#)]
- Li, J.; Zhang, W.; Xu, K.; Monteiro, P.J. Fibrillar calcium silicate hydrate seeds from hydrated tricalcium silicate lower cement demand. *Cem. Concr. Res.* **2020**, *137*, 106195. [[CrossRef](#)]

22. Yu, Y.G.; Angel, R.J.; Ross, N.L. Pressure impact on the structure, elasticity, and electron density distribution of  $\text{CaSi}_2\text{O}_5$ . *Phys. Rev. B Condens. Matter Mater. Phys.* **2013**, *87*, 184112. [[CrossRef](#)]
23. Schoenitz, M.; Navrotsky, A.; Ross, N. Enthalpy of formation of  $\text{CaSi}_2\text{O}_5$ , a quenched high-pressure phase with pentacoordinate silicon. *Phys. Chem. Miner.* **2001**, *1*, 57–60. [[CrossRef](#)]
24. Rostásy, F.; Weiß, R.; Wiedemann, G. Changes of pore structure of cement mortars due to temperature. *Cem. Concr. Res.* **1980**, *10*, 157–164. [[CrossRef](#)]
25. Wang, S.; Abdulridha, A.; Naito, C.; Quiel, S.; Suleiman, M.; Romero, C.; Neti, S. Enhancement of conventional concrete mix designs for sensible thermal energy storage applications. *J. Energy Storage* **2023**, *61*, 106735. [[CrossRef](#)]
26. McNeill, I.; Sadeghi, S. Thermal Stability and Degradation Mechanisms of Poly(Acrylic Acid) and its Salts: Part 2 Sodium and Potassium Salts. *Polym. Degrad. Stab.* **1990**, *30*, 213–230. [[CrossRef](#)]
27. Aslani, F.; Jowkarmeimandi, R. Stress-strain model for concrete under cyclic loading. *Mag. Concr. Res.* **2012**, *64*, 673–685. [[CrossRef](#)]
28. Kumar, D.; Alam, M.; Zou, P.X.W.; Sanjayan, J.G.; Memon, R.A. Comparative analysis of building insulation material properties and performance. *Renew. Sustain. Energy Rev.* **2020**, *131*, 110038. [[CrossRef](#)]
29. Abu-Jdayil, B.; Mourad, A.-H.; Hittini, W.; Hassan, M.; Hameedi, S. Traditional, state-of-the-art and renewable thermal building insulation materials: An overview. *Constr. Build. Mater.* **2019**, *214*, 709–735. [[CrossRef](#)]
30. Hill, C.; Norton, A.; Dibdiakova, J. A comparison of the environmental impacts of different categories of insulation materials. *Energy Build.* **2018**, *162*, 12–20. [[CrossRef](#)]
31. D’Orazio, M.; Maracchini, G. An experimental investigation on the indoor hygrothermal environment of a reinforced-EPS based temporary housing solution. *Energy Build.* **2019**, *204*, 109500. [[CrossRef](#)]
32. di Filippo, R.; Possidente, L.; Tondini, N.; Bursi, O.S. Quantitative integration of fire risk with life cycle analysis of building: The case of thermal insulation. *J. Build. Eng.* **2023**, *76*, 107124. [[CrossRef](#)]
33. Maracchini, G.; D’Orazio, M. Improving the livability of lightweight emergency architectures: A numerical investigation on a novel reinforced-EPS based construction system. *Build. Environ.* **2022**, *208*, 108601. [[CrossRef](#)]
34. Posani, M.; Veiga, R.; Freitas, V. Post-Insulating traditional massive walls in Southern Europe: A moderate thermal resistance can be more effective than you think. *Energy Build.* **2023**, *295*, 113299. [[CrossRef](#)]
35. Ozger, O.B.; Girardi, F.; Giannuzzi, G.; Salomoni, V.; Majorana, C.; Fambri, L.; Baldassino, N.; Di Maggio, R. Effect of nylon fibers on mechanical and thermal properties of hardened concrete for energy storage systems. *Mater. Des.* **2013**, *51*, 989–997. [[CrossRef](#)]
36. Cook, R.A.; Hover, K.C. Mercury porosimetry of hardened cement pastes. *Cem. Concr. Res.* **1999**, *29*, 933–943. [[CrossRef](#)]
37. Zhou, J.; Ye, G.; van Breugel, K. Characterization of pore structure in cement-based materials using pressurization–depressurization cycling mercury intrusion porosimetry. *Cem. Concr. Res.* **2010**, *40*, 1120–1128. [[CrossRef](#)]
38. Lange, D.A.; Jennings, H.M.; Surenda, S.P. Image analysis techniques for characterization of pore structure of cement-based materials. *Cem. Concr. Res.* **1994**, *24*, 841–853. [[CrossRef](#)]
39. Rouquerol, J.; Avnir, D.; Fairbridge, C.W.; Everett, D.H.; Haynes, J.H.; Pernicone, N.; Ramsay, J.D.F.; Sing, K.S.W.; Unger, K.K. Recommendations For The Characterization Of Porous Solids (Technical Report). *Pure Appl. Chem.* **1994**, *66*, 1739–1758. [[CrossRef](#)]
40. Nurazuwa, M.; Munadrah; Irmawaty, R.; Muhiddin, A. Compressive strength and microstructure of self-compacting concrete with nylon fiber substitution. *IOP Conf. Ser. Earth Environ. Sci.* **2022**, *1117*, 012016. [[CrossRef](#)]
41. Shalchy, F.; Rahbar, N. Nanostructural characteristics and interfacial properties of polymer fibers in cement matrix. *ACS Appl. Mater. Interfaces* **2015**, *7*, 17278–17286. [[CrossRef](#)]
42. Jenkins, M.G.; Lara-Curzio, E.; Ashbaugh, N.E. *Thermal and Mechanical Test Methods and Behavior of Continuous-Fiber Ceramic Composites*; ASTM International: West Conshohocken, PA, USA, 1997; Volume 1309.
43. Ashby, M.F. *Materials Selection in Mechanical Design*, 3rd ed.; Butterworth-Heinemann: Oxford, UK, 2005.
44. Girardi, F.; Giannuzzi, G.; Mazzei, D.; Salomoni, V.; Majorana, C.; Di Maggio, R. Recycled additions for improving the thermal conductivity of concrete in preparing energy storage systems. *Constr. Build. Mater.* **2017**, *135*, 565–579. [[CrossRef](#)]
45. Ali, S.I.A.; Lublo, E. Effect of elevated temperature on the magnetite and quartz concrete at different  $w/c$  ratios as nuclear shielding concretes. *Nucl. Mater. Energy* **2022**, *33*, 101234.
46. Zhang, X.; Liu, W.; Cao, M.; Zhang, S.; Hou, J. Performances of heat-insulating concrete doped with straw fibers for use in tunnels. *Buildings* **2023**, *13*, 818. [[CrossRef](#)]
47. Gencil, O.; Harja, M.; Sari, A.; Hekimog, G.; Ustaog, A.; Sutcu, M.; Erdogmus, E.; Kaplan, G.; Bayraktar, O.Y. Development, characterization, and performance analysis of shape-stabilized phase change material included-geopolymer for passive thermal management of buildings. *Int. J. Energy Res.* **2022**, *46*, 21841–21855. [[CrossRef](#)]
48. Charai, M.; Mezrhab, A.; Moga, L.; Karkri, M. Hygrothermal, mechanical and durability assessment of vegetable concrete mixes made with alfa fibers for structural and thermal insulating applications. *Constr. Build. Mater.* **2022**, *335*, 127518. [[CrossRef](#)]
49. Jia, H.; Cui, B.; Niu, G.; Chen, J.; Yang, Y.; Wang, Q.; Tang, C. Experimental and mechanism study on the impermeability and thermal insulation of foam concrete regulated by nano-silica and fluorine-free foam. *J. Build. Eng.* **2023**, *64*, 105675. [[CrossRef](#)]

**Disclaimer/Publisher’s Note:** The statements, opinions and data contained in all publications are solely those of the individual author(s) and contributor(s) and not of MDPI and/or the editor(s). MDPI and/or the editor(s) disclaim responsibility for any injury to people or property resulting from any ideas, methods, instructions or products referred to in the content.